Available online at www.sciencedirect.com
SCIENCE DIRECT®
Journal of Nuclear Materials 334 (2004) 1–8
journal of nuclear materials
www.elsevier.com/locate/jnucmat

Electronic structure of UC_x films prepared by sputter co-deposition

M. Eckle [a], R. Eloirdi [a], T. Gouder [a,*], M. Colarieti Tosti [a,b], F. Wastin [a], J. Rebizant [a]

[a] European Commission, Joint Research Centre, Institute for Transuranium Elements, P.O. Box 2340, D-76175 Karlsruhe, Germany
[b] Department of Physics, Uppsala University, P.O. Box 530, SE-751 21 Uppsala, Sweden

Received 3 September 2003; accepted 17 March 2004

Abstract

Thin layers of UC_x ($x = 0$–12) have been prepared by sputter co-deposition of uranium and carbon in an Ar atmosphere. The films were investigated in-situ by ultraviolet and X-ray photoelectron spectroscopy (UPS and XPS, respectively). Special interest was put on the evolution of the electronic structure with the composition of the films, as deduced from the U-4f, C-1s and valence region spectra. With increasing carbon content, three types of carbon species were detected according to C-1s core level line, at 282, 282.6 and 284.5 eV binding energy (BE). They are attributed to the UC, UC_2 and graphite phases, respectively. The U-4f core levels do not change strongly with increasing carbon content, showing well-itinerant U-5f electrons. Similarly, valence region spectra show three types of carbon species for different UC_x films, which are differentiated by their C-2p signals. A strong hybridisation between C-2p and U-5f states is detected in UC, while the C-2p signal in UC_2 appears only weakly hybridised, and for higher carbon contents a π band characteristic of graphite appears.

1. Introduction

Uranium carbides are important materials in nuclear research. They are being considered as advanced fuels for generation IV reactors (as solid solutions of uranium and one or more refractory metal carbides) [1]. Also, uranium carbides are currently used as fission targets in spallation sources [2]. They are discussed as possible fuel for fast breeder reactors [3]. More recently mixed uranium/refractory metal carbide fuels are suggested as high performance nuclear propellants in space exploration applications [4]. Carbides are chosen because of their high heat conductance, density, high melting points and thermodynamic stability. Decomposition, interdiffusion with their surrounding, or surface corrosion are important issues for the practical handling of these advanced fuels or storage of the corresponding waste.

In this paper we present a photoemission study of the electronic structure of uranium carbide films with varying composition. Thin films were prepared by sputter co-deposition from uranium and graphite targets. We used mainly photoemission but also X-ray diffraction (XRD) to characterize the compounds. One question was whether all the three uranium carbide compounds (UC, U_2C_3 and UC_2) [5] could be obtained by our method.

While bulk uranium monocarbide (UC) has been studied by photoemission [6], no data are available for the higher carbides. This was a second motivation for studying U carbide films. We are interested in the evolution of the electronic structure of U within the carbide series, where U atoms are diluted in a carbon matrix. The 5f orbitals are only weakly overlapping, and form

* Corresponding author. Tel.: +49-7247 951243; fax: +49-7247 951599.
E-mail address: gouder@itu.fzk.de (T. Gouder).

0022-3115/$ - see front matter © 2004 Elsevier B.V. All rights reserved.
doi:10.1016/j.jnucmat.2004.03.007

narrow bands of highly correlated states. These states confer a series of interesting physical (magnetism, superconductivity [7]) and chemical (mixed and intermediate valence [8]) properties to the actinide compounds. While in concentrated metallic compounds, the direct f–f overlap dominates and ensures bonding (delocalization) of the f states, dilution (e.g. in a carbon matrix) may push the f states into localization. Above a critical interactinide spacing, the Hill-limit (0.354 nm for U), direct f–f overlap becomes negligible. For such materials, f bonding is only possible via hybridisation of the f states with states of the ligands, resulting in an increased tendency for their localization [9]. This should be especially pronounced when the uranium atoms are strongly diluted, i.e., atomically isolated. This can be done by co-depositing uranium and the matrix element (in this case carbon), when even highly diluted non-stoichiometric compositions can be prepared. It must be emphasized, however, that this is successful if the films remain homogeneous and no phase separation takes place. This is often the case for alloys, where intermediate compositions can be prepared, because of the fast cooling rate of the impinging atoms that allows quenching metastable phases. However, for compounds, there is an increased tendency for dismutation into mixtures of stable phases. This may preclude tuning of the spacing. In uranium carbides the U–U separation varies only slightly from UC (0.350 nm) to UC_2 (0.354 nm) and U_2C_3 (0.334 nm). All values are close to the Hill-limit (0.354 nm) and, a priori, 5f delocalization should be expected. But it is an interesting question whether the U-5f states could become localized for highly diluted uranium atoms in a carbon matrix.

2. Experimental

Thin films of UC_x were prepared in-situ by DC co-sputtering of U and graphite. As sputter gas, we used high purity (99.99%) Ar at a pressure of 5×10^{-5} Pa. The deposition rates of U and C were controlled by varying the voltage of the U target (−100 to −900 V) and graphite target (−100 to −700 V). The plasma in the diode source was maintained by injecting electrons of 50–100 eV kinetic energy. Shields were installed to expose only the sample to the Ar–U–C plasma and kept the targets contamination of the chamber as low as possible. The U target was a U metal disc (99.99% of purity, 5 mm radius, 1 mm thickness) and the C target was a graphite high purity rod (99.99%, 1.5 mm radius). Both targets were kept at room temperature by air-cooling. The deposition rates were about 0.1 nm s^{-1}. For photoemission measurements films of 20 nm thickness were deposited at room temperature on a single crystalline Si(1 1 1) wafer. The background pressure of the plasma chamber was 1.3×10^{-8} Pa.

Photoemission data were recorded in-situ using a Leyboldt LHS-10 hemispherical analyser. XPS spectra were taken using MgKα (1253.6 eV) radiation with an approximate resolution of 0.9 eV. UPS measurements were made using He I and He II (21.22 and 40.81 eV) excitation radiation, produced by a windowless UV rare gas discharge source. The total resolution in UPS was 0.1–0.05 eV for the high resolution scans. The background pressure in the analysis chamber was 2.6×10^{-8} Pa. The XRD measurements were made on a conventional Phillips PW3830 powder-diffractometer with a Cu anode (λ K$\alpha_1 = 0.1540560$ nm). Films of 120 nm thickness were deposited at ambient temperature and 200 °C on a quartz glass substrate. The assignation of the peaks has been made using PCPDFwin database.

3. Results

UC_x films were prepared in a wide concentration range. The composition of the films was determined from the U-4f/C-1s intensity ratios. In absence of carbon (graphite target set to ground potential), high purity U metal films with less than 2 at.% oxygen were prepared. In absence of U (U target set to ground potential), almost pure graphite films (containing 2 at.%U) were deposited. The carbide films were labelled as UC_x, instead of the more generally used U_aC_b (a and b given in at.%). This does not imply the formation of well-defined phases for the films but it is used for easier comparison between the films and the stoichiometric bulk compounds (UC, U_2C_3 and UC_2).

We first discuss the C-1s and the U-4f core levels to obtain information about carbide species and the localization–delocalization of the U-5f electrons. Then we address the evolution of the valence band region, which was observed by UPS. In a third part, we present the crystalline structure of $UC_{1.2}$ and $UC_{1.6}$ films as determined by XRD.

3.1. C-1s core level

Fig. 1 shows characteristic C-1s core level spectra of UC_x thin films. Three carbon species are observed at different binding energies (BE), and noted ^{1}C, ^{2}C and ^{3}C. The C-1s line (^{1}C) for a film composition of $UC_{0.8}$ has a binding energy of 282.0 eV. This is close to the published values for bulk transition metal-carbides (MC) [10] and UC [11]. We notice that the width of the C-1s peak increases from substoichiometric UC_{1-x} to stoichiometric UC. This has also been observed for other carbide compounds and assigned to bulk and surface vacancies present in the films [12]. At higher C contents, a new C-1s line appears at 282.6 eV (^{2}C), replacing ^{1}C for a C content of UC_2. ^{1}C and ^{2}C can thus be correlated to the carbon species present in UC and

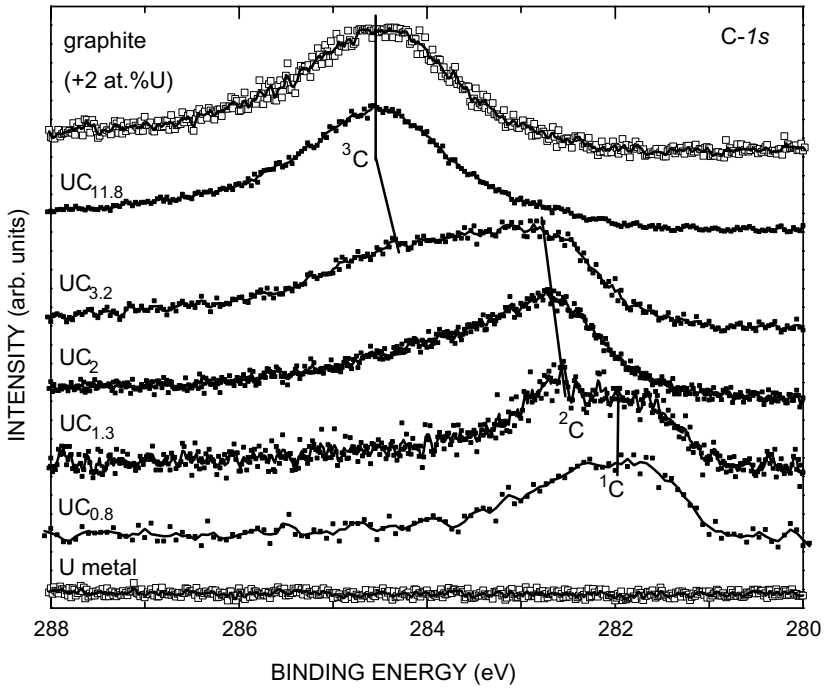

Fig. 1. C-1s spectra of UC_x films compared to U metal and graphite (+2 at.%U) films. Three carbon species, identified as (^{1}C), (^{2}C) and (^{3}C), are attributed to UC, UC_2 and graphite, respectively.

UC_2 compounds. The ^{1}C and ^{2}C signals superpose in $UC_{1.3}$. We will discuss below the reason for the different binding energy, which is directly related to the electronic structure of the carbides. A third C-1s peak labelled ^{3}C appears at even higher carbon content. Its binding energy of about 284 eV is close to that of graphite (284.5 eV), which points to a similar electronic structure. The ^{2}C and ^{3}C signals co-exist in $UC_{3.2}$. Thus, $UC_{3.2}$ is not a well-defined compound but rather a mixture of UC_2 and graphite. With increasing carbon content both ^{2}C and ^{3}C lines shift towards higher BE. The ^{3}C line eventually reaches 284.5 eV, which is the value of graphitic carbon.

3.2. U-4f core level

Fig. 2 shows the U-4f core levels, split by the spin–orbit interaction into the $4f_{5/2}$ and $4f_{7/2}$ components. Their binding energies (377.3 eV for U-$4f_{7/2}$) are consistent with literature values [13]. Introduction of carbon leads to a slight shift of U-4f lines toward higher BE and to a broadening of the peaks. The shift is about 0.6 eV in $UC_{0.8}$. The U-$4f_{7/2}$ binding energy in $UC_{0.8}$ ($\approx$377.9 eV) is identical with that found for UC bulk [11,14]. Also the small satellite, which appears at 6 eV higher binding energy, has been observed in UC. It is attributed to shake-up feature due to charge transfer from the filled U-5f states into the empty C ligand 2p states [11]. Further introduction of carbon does not influence the U-4f lines; binding energy and shape of the U-4f lines remain virtually identical up to UC_2. This strongly contrasts to the pronounced evolution of the C-1s lines. The U-4f lines further broaden in $UC_{3.2}$ and $UC_{11.8}$, developing supplementary intensity on the high binding energy side. Then, we deposited graphite alone (with the U metal target set to zero voltage). This film still contained small amounts of uranium, about 2 at.%, due to cross-contamination of the graphite target. The U-4f lines of this film appear as broad peaks having two components labelled **P** and **W**, also visible in $UC_{11.8}$. These two components appear in U compounds, where the 5f electrons are close to localization [15]. They are due to the co-existence of two different final states after ejection of the photoelectron in these systems. The photohole in uranium is screened either by occupation of an empty f or an empty d state. Filling of f state provides more efficient screening, because the f orbitals are smaller than the d orbitals and thus place the screening charge closer to the core hole. This leads to the existence of well (**W**)(f) and poorly (**P**)(d) screened final states. In most metallic U compounds the f states are itinerant and the f screened final state (**W**) dominates. Only in those U compounds, were the f-states become localized the d screened (**P**) becomes important (e.g. UPd_3 [16]). The appearance of peak **P** for $UC_{11.8}$ and U/graphite thus provides a clear hint, that the 5f electrons of U atoms dispersed in a graphite matrix become indeed localized and no longer

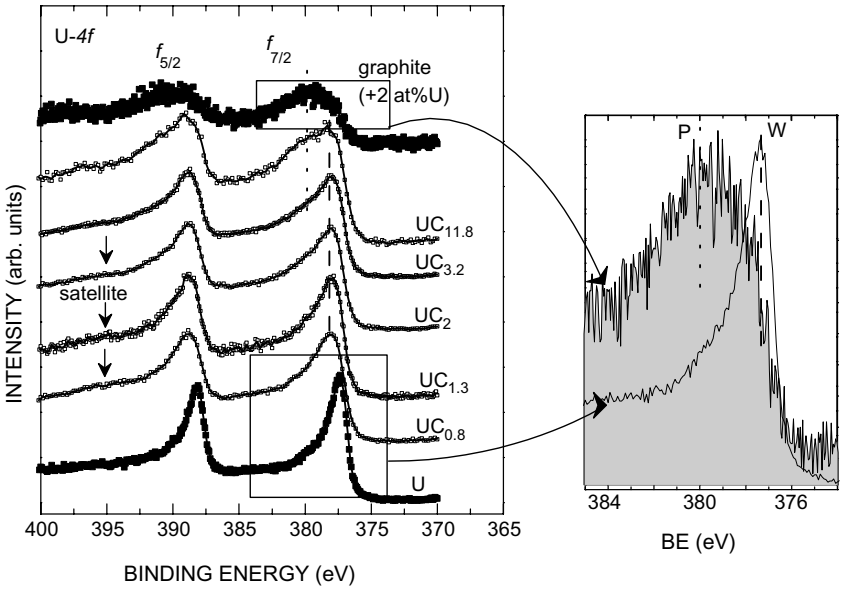

Fig. 2. U-4f spectra of UC_x films compared to U metal and graphite films.

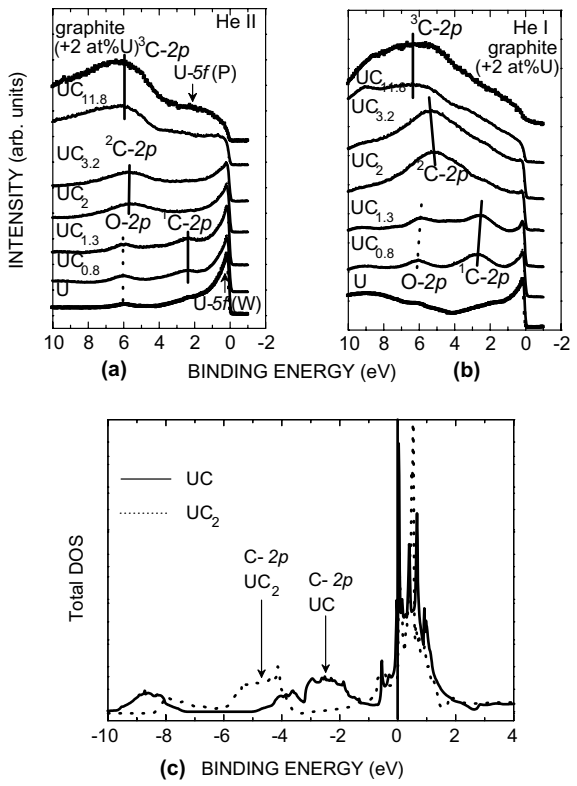

Fig. 3. (a) He II spectra of UC_x films compared to U metal and graphite (+2 at.%U) films. (b) He I spectra of UC_x films compared to U metal and graphite (+2 at.%U) films. (c) Calculated total density of state (DOS) of UC and UC_2.

participate in the chemical bonding. It should be noticed that the presence of oxygen contaminations also could produce a photoemission line at the position of **P**, if UO_2 is formed (with a U-4$f_{7/2}$ signal at 380.0–381.0 eV). However, UPS shows that the films are virtually oxygen free (see below). In addition, in presence of carbon, these small amounts of oxygen would form an oxycarbide, as shown in previous work [17].

3.3. UPS study

Valence band spectra have been taken using He I and He II radiation (Fig. 3(a) and (b)). Comparison of He I and He II spectra helps identifying the photoemission lines, because the cross-sections of the various sublevels (s, p, d, f) have different energy dependence (Table 1). Pure U metal has a strong, sharp emission at the Fermi level, which is ascribed to the conduction band formed by itinerant 5f states [18]. The weak peak at 2 eV is generally attributed to the U-6d states, hybridised with the 5f states [19]. The emission at 6 eV is due to some oxygen contamination. It is more pronounced in He I than in He II because of the enhanced O-2p and

Table 1
Atomic subshell photoionization cross-sections σ of carbon, uranium and oxygen in He I and He II

σ	O-2p	C-2p	C-2s	U-5f	U-6d
He I	10.67	6.13	1.23	0.64	4.01
He II	6.82	1.87	1.17	6.05	0.68

the reduced U-5f cross-sections in He I (Table 1). It corresponds to about 2 at.% oxygen on the top surface. In $UC_{0.8}$, a new peak appears at about 2.2 eV BE in He II and 2.8 eV in He I. This line has also been observed in UC [11] and attributed to the C-2p valence band (^{1}C-2p). ^{1}C-2p signal is more intense for the $UC_{1.3}$ film. The 2p character of this peak is corroborated by the increased intensity in He I, typical for the C-2p cross-section. With further addition of carbon to UC_2, the ^{1}C-2p signal is replaced by a C-2p emission at about 5 eV (^{2}C-2p). At even higher carbon concentrations ($UC_{11.8}$), the ^{2}C-2p peak broadens and shifts to become similar to that of graphite (^{3}C-2p). The evolution of the C-2p lines is thus reminiscent of that of the C-1s line, where ^{1}C in UC is replaced by ^{2}C in UC_2 and eventually by a graphite-like ^{3}C in $UC_{11.8}$. The total densities of states (DOS) of UC and UC_2 (Fig. 3(b)) were obtained with self-consistent band structure calculations within the local density approximation (LDA) [20] to the density functional theory [21] in the parameterisation of [22]. The electronic structure calculations used the efficient linear muffin-tin orbital [23] technique. The potential is assumed to be spherical inside each muffin-tin sphere (atomic sphere approximation). The crystal structures considered are fcc for UC with a lattice parameter of $a = 0.4962$ nm and tetragonal I4/mmm for UC_2 with a lattice parameter of $a = 0.3517$ nm and $c = 0.5987$ nm [24]. U-5f electrons are free to hybridise and both systems studied are only considered in their paramagnetic phase. The Brillouin zone sampling in both cases here reported is done with a 1000 k-points mesh (10 10 10). A comparison with the results obtained with a mesh of only 125 k-points (5 5 5) showed that our calculations are convergent. The calculations showed C-2p valence band peaks in UC (2.5 eV) and UC_2 (5 eV). These peaks correspond well to the C-2p photoemission peaks (Fig. 3(a)). Thus, there is very good agreement between measured and calculated DOS in UC and UC_2.

In all carbide films, with the exception of the highly diluted U-graphite (2 at.%U), the U-5f line remains pinned at the Fermi level. This shows that in all cases, the 5f states are itinerant [25]. This is in agreement with the temperature-independent paramagnetic (TIP) behaviour of UC, U_2C_3, and UC_2, excluding the presence of a local magnetic moment. U_2C_3 exhibits itinerant magnetism only at low temperature [25]. With increasing carbon contents, the 5f peak decreases in intensity, because of the lowered uranium concentration. Its intensity is also suppressed in He I, as expected from the cross-sections (Table 1). In U-graphite (2 at.%U), the peak at the Fermi level disappears completely. It is replaced by a long plateau between 0.5 and 3 eV. Pure graphite (Fig. 4) does not have such a plateau, but instead a continuously decreasing intensity. The difference spectrum (Fig. 4) allows separating the uranium and the graphite features. It shows a U peak centred at 1 eV binding energy. Similar signals have been observed for U systems with localized f electrons, such as UPd_3 [25] and $U(Pd,Pt)_x$ [26]. This provides a clear indication, that the U atoms at high dilutions eventually have local-

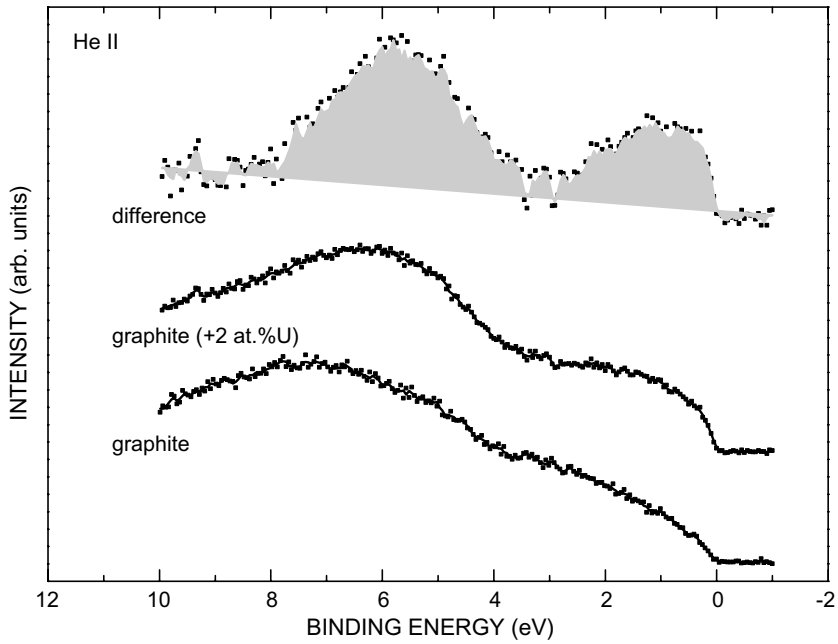

Fig. 4. Comparison of He II valence band spectra of pure graphite and graphite (+2 at.%U). The difference between the two spectra is also shown.

ized 5f states. The peak around 6 eV binding energy corresponds to the π band of graphite [27]. The introduction of electropositive U atoms into a graphite matrix can affect the π band of graphite. This feature can be related to the shift of ^{3}C to higher BE.

3.4. XRD study

XRD measurements were carried out on $UC_{1.2}$ and $UC_{1.6}$ film (Fig. 5). The films were deposited on a quartz glass support, whose XRD pattern is shown for reference. The $UC_{1.2}$ film (Fig. 5(a)) is close in stoichiometry to UC. For this film we observed an intense peak corresponding to the (1 1 1) plane of the UC phase (PDF: 73–1709), and a weak peak assigned to the (2 1 1) plane of U_2C_3 (PDF: 74–0805). There is thus predominance of a strongly textured UC phase. The peaks are wide, suggesting small crystallite size. Stress and inhomogeneities of the films could also contribute to the broadening [28] and could be responsible for the small shift of the peaks away from the ideal Bragg peak positions [29]. Uranium sesquicarbide is known to co-exist with UC [30] and to decompose into UC and UC_2 at ambient temperature [31]. In addition, thermal analysis studies of the U–C phase diagram showed, that the formation of U_2C_3 is possible in the range of $UC_{1.1}$ to $UC_{1.5}$ [32] at elevated temperatures. The high cooling rate of surface layers during the deposition may explain the formation of high temperature phases frozen at room temperature.

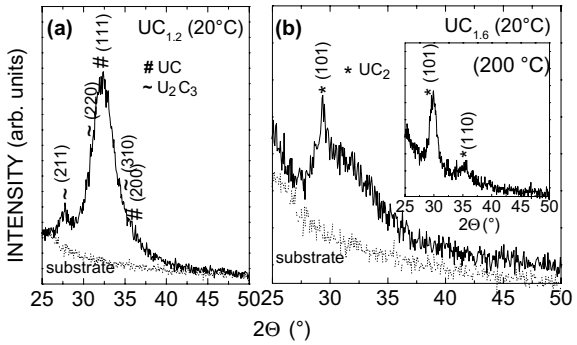

Fig. 5. (a) XRD of a $UC_{1.2}$ film (full line) deposited on a Si (quartz glass) substrate at room temperature (dotted line) shows a UC phase (PDF: 73–1709) and a weak peak assigned to the (2 1 1) plane of U_2C_3 (PDF: 74-0805). (b) XRD of a $UC_{1.6}$ film (full line) deposited at room temperature and at 200 °C (see inset) show the (1 0 1) reflection of the UC_2 phase (PDF: 84–1344). The film deposited at 200 °C is more crystalline. The XRD pattern of the quartz glass substrate is given as reference.

The XRD pattern of the $UC_{1.6}$ film (Fig. 5(b)) shows the (1 0 1) reflection of the UC_2 phase (PDF: 84–1344). Again, there are no other reflections pointing to the preferential orientation of the film. A broad background peak around 33° (2Θ) indicates the presence of an amorphous phase. The introduction of additional carbon into the lattice may create more disorder in the matrix and thus favour amorphisation. A $UC_{1.6}$ film deposited on a substrate heated to 200 °C showed better crystallographic order (inset Fig. 5(b)). The amorphous phase disappeared and a strong (1 0 1) diffraction peak of the UC_2 phase is observed. Thus deposition at elevated temperature resulted in larger crystallites. The (1 0 1) and (1 1 0) diffraction peaks of the UC_2 phase are now clearly observed and in good agreement with the literature [33,34].

4. Discussion

4.1. Formation of the different carbide phases

Uranium–carbon films were prepared in a wide U/C concentration range. A central question was, whether we really formed the three carbide compounds, UC, U_2C_3 and UC_2. The C-1s core level and C-2p valence band are very sensitive to the composition. This is directly related to the differences in the electronic structure of the carbides and can be used as diagnostic tool for identification of the phases. The structure and chemical environment of the carbon atoms change for the different carbides (Fig. 6). The carbon atoms in UC (cubic,

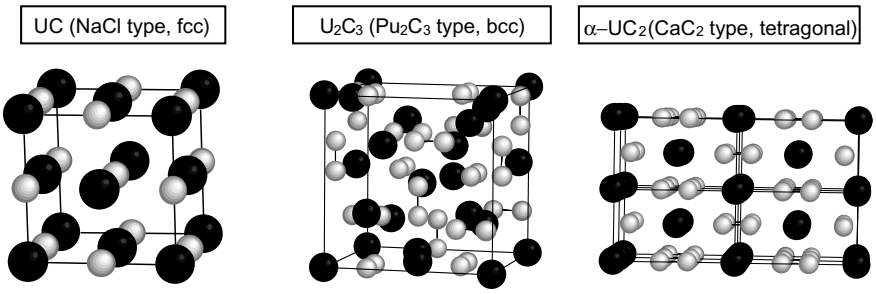

Fig. 6. Crystalline structure of UC, U_2C_3 and UC_2.

NaCl structure) are well-separated from each other and direct C–C interaction is weak. There is a strong hybridisation between the C-2p and U-5f states [35]. The valence band, with mainly C-2p character, is located at 2 eV as consistently shown by UPS (Fig. 3(a)) and band structure calculations (Fig. 3(b)). The C atoms in the dicarbide (tetragonal, CaC_2 structure) are substituted by C–C dimers. By this interaction the C-2p atomic orbitals are split into bonding and antibonding molecular orbitals [36]. The bonding molecular orbital, which lies at higher binding energy than the atomic orbital, hybridizes with the U states. It gives the C-2p valence band of UC_2, and the high BE shift in the dicarbide compared to the monocarbide can be related to the molecular orbital in the dimer (Fig. 3(a) and (b)).

Like the dicarbide, the sesquicarbide contains only carbon dimers, and the C–C distances in these dimers are even shorter than in the dicarbide (0.1295 nm versus 0.1340 nm [37]). Due to the similarity in the electronic structure we can expect similar behaviour of the photoemission lines. So it is questionable, whether photoemission signals of the sesquicarbide and dicarbide are distinguishable. As an example the C-1s photoemission of $UC_{1.3}$ (Fig. 1) can be discussed. The signal may be interpreted as superposition of the ^{1}C line of UC and the ^{2}C line of UC_2 in a ratio of 70/30 at.%, which would perfectly account for the composition of $UC_{1.3}$. It is also possible to express $UC_{1.3}$ as a mixture of U_2C_3 and UC (40/60 at.%). In this case the ^{2}C would be due to the sesquicarbide (i.e. the same binding energy for sesquicarbide and dicarbide). But the matching with the intensity of the photoemission signal is much worse. Also other interpretations are possible (e.g. two C-1s lines for the sesquicarbide), but this discussion becomes speculative. So it should be concluded that photoemission is not capable of proving the formation of sesquicarbide, but the data may be perfectly attributed to a mixture of UC and UC_2. The only indication for U_2C_3 formation comes from XRD, which shows a weak sesquicarbide signal. But here the problem is that XRD detects only the crystalline part and an amorphous sesquicarbide would not be detected. Finally, it has been shown that the preparation of sesquicarbide by classical bulk synthesis methods is difficult. Systems of a formal U_2C_3 composition consist in reality of a mixture of UC and UC_2 [3]. The phase diagram shows that U_2C_3 is stable only in a temperature range extending from 1100 to 1500 °C. At lower temperatures it decomposes into UC and C, and at higher temperatures UC_2 and UC are formed. Annealing at well-chosen temperatures is necessary to convert the mixtures into sesquicarbide, and this conversion is never complete. The particles come from a high temperature phase (the plasma) by sputter deposition and are instantaneously fixed on the surface. The surface would thus show rather a frozen high-temperature phase, and this would be the mixture of UC_2 and UC.

4.2. Localization of the U-5f states

Do isolated uranium atoms in a carbon matrix have localized 5f states? Atomic isolation favours indeed such localization, if there is no strong interaction of the 5f states with their environment (ligand effect), which in turn would favour again delocalization. Does such interaction exist in the U–C system? This question has been addressed in U – graphite intercalation compounds (GIC), where U atoms are embedded between the graphite layers [27]. In U – GICs the U–U distances are large, and band structure calculations indicate a transition of the 5f states from itinerant to localized behaviour. The U-5f emission is situated at the Fermi level and does not disperse (as it would be if it was a broad band). On the other side, no multiplet features are observed, as would be expected for classical localized systems. The conclusion is that these are intermediate valence systems, where the weakly localized 5f states still are exchanging electrons with the conduction band (thus valence fluctuations). This would allow reconciling the position at the Fermi level with the absence of dispersion and multiplet. In our case, even more diluted systems are produced (containing 2 at.% uranium) and the long-range order of graphite-intercalation systems is missing. This favours 5f localization. Indeed, we do observe signs of a stronger localization: in the core level the poorly screened peak eventually becomes dominant (Fig. 2) and the 5f peak moves away from the Fermi level (Fig. 4). The 5f emission looks similar to that in UPd_3, which is the classical U alloy system with localized 5f electrons [16].

5. Conclusions

Thin films of uranium carbides were prepared by sputter co-deposition of uranium and graphite. UC and UC_2 formation was shown by photoemission spectroscopy, theoretical band structure calculations and X-ray diffraction. U_2C_3 formation was ambiguous. Photoemission data were not conclusive while XRD showed a weak reflection of the U_2C_3 phase. The carbon signals (C-1s and C-2p) strongly changed for UC and UC_2, which was attributed to the different carbon forms (atomic carbon in UC, C–C dimers in UC_2. The U signal did not change, except for highest dilutions. U atoms kept itinerant f electrons, and only at highest dilutions (2 at.%U) the 5f states became localized.

Sputter deposition thus is a convenient method for preparing small quantities of UC and UC_2, e.g., for spectroscopic studies.

Acknowledgements

We thank F. Huber for the technical support to this work and M.S.S. Brooks for fruitful discussions. M. Eckle, M. Colarieti Tosti and R. Eloirdi acknowledge the European Commission for support in the frame of the program 'Training and Mobility of Researchers'.

References

[1] Generation IV roadmap, US DOE nuclear energy research advisory committee and the generation iv international forum, report GIF-002-00, 2000, http://gif.inel.gov/roadmap.
[2] E. Hagebo, P. Hoff, O.C. Jonsson, E. Kugler, J.P. Omtvedt, H.L. Ravn, K. Steffensen, Nucl. Instrum. and Meth. B 70 (1992) 165.
[3] H. Holleck, H. Kleykamp, in: Gmelin Handbook of Inorganic Chemistry, Uranium Suppl. vol. C12, Springer, Berlin, 1987.
[4] T.W. Knight, S. Anghaie, J. Nucl. Mater. 306 (2002) 54.
[5] P.Y. Chevalier, E. Fischer, J. Nucl. Mater. 288 (2001) 100.
[6] T. Ejima, K. Murata, S. Suzuki, T. Takahashi, S. Sato, T. Kasuya, Y. Onuki, H. Yamagami, A. Hasegawa, T. Ishii, Physica B 186 (1993) 77.
[7] J.M. Fournier, L. Manes, Actinides-Chemistry and Physical Properties, Structure and Bonding, vol. 59&60, Springer, Berlin, 1985.
[8] P. Wachter, M. Filzmoser, J. Rebizant, Physica B 293 (2001) 199.
[9] D.D. Sarma, S. Krummacher, F.U. Hillebrecht, D.D. Koelling, Phys. Rev. B 38 (1988) 1.
[10] L.I. Johansson, Surf. Sci. Rep. 21 (1995) 177.
[11] J.G. Dillard, H. Moers, H. Klewe-Nebenius, G. Kirch, G. Pfennig, H.J. Ache, J. Phys. Chem. 88 (1984) 5345.
[12] G.H. Schadler, Solid State Commun. 74 (1990) 1229.
[13] J.F. Moulder, W.F. Stickle, P.E. Sobol, K.D. Bomben, in: J. Chastain (Ed.), Handbook of X-Ray Photoelectron Spectroscopy, Perkin-Elmer Corporation Physical Electronic Division, USA, 1992.
[14] T. Ejima, S. Sato, S. Suzuki, Y. Saito, S. Fujimori, N. Sato, M. Kasaya, T. Komatsubara, T. Kasuya, Y. Onuki, T. Ishii, Phys. Rev. B 53 (1996) 1806.
[15] J.R. Naegele, J. Ghijsen, L. Manes, Actinides-Chemistry and Physical Properties, Structure and Bonding, vol. 59&60, Springer, Berlin, 1985.
[16] Y. Baer, H.R. Ott, K. Andres, Solid State Commun. 36 (1980) 387.
[17] T. Gouder, C.A. Colmenares, J.R. Naegele, J.C. Spirlet, J. Verbist, Surf. Sci. 264 (1992) 354.
[18] M. Iwan, E.E. Koch, F.-J. Himpsel, Phys. Rev. B 24 (1981) 613.
[19] S.L. Molodtsov, J. Boysen, M. Richter, P. Segovia, C. Laubschat, S.A. Gorovikov, A.M. Ionov, G.V. Prudnikova, V.K. Damchuk, Phys. Rev. B 57 (1998) 13241.
[20] W. Kohn, L.J. Sham, Phys. Rev. A 140 (1965) 1133.
[21] P. Hohenberg, W. Kohn, Phys. Rev. B 136 (1964) 864.
[22] S.J. Vosko, L. Wilk, M. Nusair, Can. J. Phys. 58 (1980) 1200.
[23] O.K. Andersen, Phys. Rev. B 12 (1975) 3060.
[24] D.W. Jones, I.J. McColm, R. Steadman, J. Yerkess, J. Solid State Chem. 68 (1987) 219.
[25] B. Reihl, N. Martensson, D.E. Eastman, A.J. Arko, O. Vogt, Phys. Rev. B 26 (1982) 1842.
[26] A.J. Arko, D.D. Koelling, C. Capasso, M. del Giudice, C.G. Olson, Phys. Rev. B 38 (1988) 1627.
[27] S. Danzenbächer, S.L. Molodtsov, J. Boysen, C. Laubschat, A.M. Shikin, A. Gorovikov, M. Richter, Phys. Rev. B 64 (2001) 35404.
[28] J.G.M. Van Berkum, A.C. Vermeulen, R. Delhez, T.H. de Keijser, E.J. Mittemeijer, J. Appl. Cryst. 27 (1994) 345.
[29] R. Delhez, T.H. de Keijser, E.J. Mittemeijer, Fresenius Z. Anal. Chem. 312 (1982) 1.
[30] M.B. Sears, L.M. Ferris, J. Nucl. Mater. 32 (1969) 101.
[31] A. Buschinelli, A. Naoumidis, H. Nickel, J. Nucl. Mater. 58 (1975) 67.
[32] R. Benz, C.G. Hoffmann, G.N. Ruppert, High Temp. Sci. 1 (1969) 342.
[33] E. Pascalini, Carbon 35 (1997) 783.
[34] R. Arkush, M.H. Mintz, G. Kimmel, N. Shamir, J. Alloys Comp. 340 (2002) 122.
[35] M.S.S. Brooks, J. Phys. F 14 (1984) 639.
[36] J. Li, R. Hoffmann, Chem. Mater. 1 (1989) 83.
[37] A.E. Austin, Acta Cryst. 12 (1959) 159.